Numerical simulation of the effect of target distance variables on vertical scour of submerged water jets

Chen Hao[1]，Teng Xian-bin[2]，Zhu Fa-xin[1]，Zhang Zhi-bin[2]，Zhang Xiao[1]

(1-College of Shipping and Maritime Transport, Zhejiang Ocean University, Zhoushan, Zhejiang 316000, China.

2-College of Marine Engineering, Guangzhou Maritime University, Guangzhou, Guangdong 510700, China.)

Keywords: submerged water jets, target distance variables, nested grids, numerical simulation, empirical formulation

ABSTRACT

Water jet technology has been increasingly applied to subsea trenching operations in recent years. In this paper, from the practical point of view of subsea salvage, based on Flow-3D fluid software, it is concluded that the calculation results obtained by using nested grid, and the error is about 13% smaller than the previous simulation results, which proves that the grid division method is feasible and credible. The target distance is an important parameter affecting water jet scouring, and in this paper, based on the nested grid, with different target distances as variables and the maximum scouring pit depth as the measurement parameter, the relationship between the target distance l and the maximum pit depth during water jet pit punching operation was investigated. And an empirical formula for the variation of pit depth with target distance in the main section under a specific condition is obtained.

1. Introduction

The shipping industry is an important pillar of China's national economy, with the continuous development of water transportation, increase in base makes the number of water wrecks also skyrocketed, timely salvage of wrecked objects is of economic and environmental importance. The water jet is a high-energy jet set obtained by using water as a raw material and passing it through a narrow nozzle under high pressure . As an emerging technical means with cleaner and more efficient characteristics, it has been widely used in the field of dredging in recent years, and many studies have been done by scholars at home and abroad.

Rouse [1] found experimentally that the velocity of the jet is the most important factor affecting the jet flushing mud. Dunn [2] found experimentally that the critical shear stress generated during the flushing process is the key to the creation of the flushing crater. N. Rajaratnam [3] studied the effect of factors such as target distance on the effect of sediment flushing. Aderibigbe [4] experimentally found the pattern of wash pit shape under the impact of vertical water jet. Liu Cheng [9] proposed three stages of scour pits by experiments. Wang Jian-jun[10] found experimentally that the maximum scour pit depth showed a logarithmic relationship with scour time. Zhang Li-shan [11] formed a submerged water jet mud flushing experimental setup can be used for the study of various types of sediment flushing methods.

The above-mentioned domestic and foreign scholars' research is mainly through physical bench tests, but there are uncertainties in the physical experiment itself such as whether the scaling ratio is reasonable, errors arising during the measurement operation, and the influence of the set-up sensors on the data. In recent years CFD software has been widely used in numerical simulation about sediment scouring. Compared with traditional bench experiments, simulation has the characteristics of low cost, high speed and high efficiency, without the existence of sensors, which can obtain data without dead ends and without affecting the simulation object itself. Liu Cheng-lin [12] used $Flow-3D$ to simulate the sediment downstream of the horizontal jet scouring fixed bottom plate, and found that the experimental results matched well by comparing and analyzing the numerical simulation and the original experiment, which proved that the sediment model in this software can be used for the analysis of the

relevant variables in physical experiments.

Target distance is an important factor affecting jet flushing[7], and a suitable target distance can make the starting effect of vertical jet and the nudging effect of horizontal diversion match well and improve the efficiency of flushing pits, so it is important to investigate the influence law of target distance variable on the effect of flushing pits. In this paper, we use Flow-3D fluid software to study the effect of different target distances l on water jet sand flushing parameters by numerical simulation, and analyze the effect of different grid divisions on simulation results.

2. Theoretical equations

The object of study in this paper is a vertically scoured submerged water jet. When the jet is vertically flushed into the sand bed, it is blocked by the sand bed, causing the original jet to reflect and diverge. The reflection flow is in the opposite direction to the original jet, and the interaction of the two forces makes the pressure increase at the critical surface of the jet and the sand bed, and the lost energy is transferred to the sand bed in the form of force, and when this force is greater than the critical starting stress of the sediment, the sediment on the surface of the sand bed starts to enter the suspended state. The diversion of the jet makes the jet flow along the surface of the sand bed to both sides, and the process will entrain the sediment that enters the suspension state together to both sides, and when it is pushed to a certain distance, the suspended sediment gradually sinks under the interaction of gravity and friction, and finally forms the scouring area of the jet.

In this paper, the Cartesian coordinate system is used and the controlling equations for water flow include the fluid continuity equation and the momentum equation.

Continuity equation.

$$\frac{\partial(uA_x)}{\partial x}+\frac{\partial(vA_y)}{\partial y}+\frac{\partial(wA_z)}{\partial z}=0 \tag{1}$$

Momentum equation.

$$\frac{\partial u}{\partial t}+\frac{1}{V_F}\left[uA_x\frac{\partial u}{\partial x}+vA_y\frac{\partial u}{\partial y}+wA_z\frac{\partial u}{\partial z}\right]=-\frac{1}{\rho}\frac{\partial p}{\partial x}+G_x+f_x-Ku \tag{2}$$

$$\frac{\partial v}{\partial t}+\frac{1}{V_F}\left[uA_x\frac{\partial u}{\partial x}+vA_y\frac{\partial u}{\partial y}+wA_z\frac{\partial u}{\partial z}\right]=-\frac{1}{\rho}\frac{\partial p}{\partial y}+G_y+f_y-Kv \tag{3}$$

$$\frac{\partial w}{\partial t}+\frac{1}{V_F}\left[uA_x\frac{\partial u}{\partial x}+vA_y\frac{\partial u}{\partial y}+wA_z\frac{\partial u}{\partial z}\right]=-\frac{1}{\rho}\frac{\partial p}{\partial z}+G_z+f_z-Kw \tag{4}$$

Where u, v, w are x, y, z the flow components in the three directions; A_x, A_y, A_z are x, y, z the fraction of area that is flowable in the three directions; V_F is the fraction of flowable volume; ρ is the density of water; p is the pressure acting on the fluid microelements; G_x, G_y, G_z is the x, y, z the acceleration of gravity in three directions; f_x, f_y, f_z for x, y, z the acceleration of viscous forces in the three directions; K is the drag increase term in the sediment transport model.

This simulation uses the $RNG\ k-\varepsilon$ model, compared to the $standard\ k-\varepsilon$ model, the RNG model corrects its analytical formula for low Reynolds number to effectively improve the accuracy of the sidewall effect, and is more suitable for solving the flow state in general[12] .

Turbulent kinetic energy k Equation.

$$\frac{\partial(\rho k)}{\partial t}+\frac{\partial(\rho k u_i)}{\partial x_i}=\frac{\partial}{\partial x_j}\left(\alpha_k\mu_{eff}\frac{\partial k}{\partial x_j}\right)+G_k-\rho\varepsilon \tag{5}$$

Dissipation rate of turbulent kinetic energy ε Equation.

$$\frac{\partial(\rho\varepsilon)}{\partial t}+\frac{\partial(\rho\varepsilon u_i)}{\partial x_i}=\frac{\partial}{\partial x_j}\left(\alpha_\varepsilon\mu_{eff}\frac{\partial\varepsilon}{\partial x_j}\right)+C_{1\varepsilon}^{*}\frac{\varepsilon}{k}G_k-C_{2\varepsilon}\rho\frac{\varepsilon^2}{k} \tag{6}$$

Where k is the turbulent kinetic energy; ε is the dissipation rate of turbulent kinetic energy; $\mu_{eff}=\mu+\mu_t$, μ is the turbulent viscosity coefficient, $\mu_t=\rho C_\mu\frac{k^2}{\varepsilon}$, $C_\mu=0.0845$; α_k and α_ε are respectively the turbulent kinetic energy and dissipation rate corresponding to the $Prandtl$ numbers, $\alpha_k=\alpha_\varepsilon=1.39$; G_k is the term for the generation of turbulent kinetic energy k, $G_k=\mu_t(\frac{\partial u_i}{\partial x_j}+\frac{\partial u_j}{\partial x_i})\frac{\partial u_i}{\partial x_j}$; $C_{1\varepsilon}^{*}=C_{1\varepsilon}-\frac{\eta(1-\eta/\eta_0)}{1+\beta\eta^3}$, $C_{1\varepsilon}$ and $C_{2\varepsilon}$ are empirical constants, $C_{1\varepsilon}=1.42$, $C_{2\varepsilon}=1.68$, $\eta_0=4.377$, $\beta=0.012$.

The controlling equations for sediment include the nudging mass transport rate equation and the suspended mass diffusion equation.

Equation for the rate of sand transport by pushing mass.

$$g_b=\rho_n\beta\left[\frac{\tau-\tau_{cr}}{\|g\|d(\rho_n-\rho)}\right]^{\frac{3}{2}}\cdot\left[\|g\|\left(\frac{\rho_n-\rho}{\rho}\right)d^3\right]^{\frac{1}{2}} \tag{7}$$

Suspended mass diffusion equation.

$$\frac{\partial C_s}{\partial t}+\nabla\left\{C_s\left[(\bar{u})+\frac{g}{\|g\|}\left[(10.36^2+1.046d_*^3)^{\frac{1}{2}}-10.36\right]\frac{v_f}{d}c_s\right]\right\}=\nabla\cdot\nabla(DC_s) \tag{8}$$

Where g_b is the bed load transport rate of bed width; ρ_n is the density of sand; β is bed load coefficient; g is the acceleration of gravity; d is the diameter of the sand; d_* is the dimensionless particle diameter of the sand; τ_{cr} is the critical bed shear; C_s is the mass concentration of suspended sediment; $\bar{u}$ is the velocity of the water-sand mixture; v_f is the kinematic viscosity coefficient of the fluid; c_s is the volume concentration of suspended sediment; D is the diffusion coefficient.

3. Model Validation

3.1 Model setup

By reading the previous literature and referring to the models of Wen Li[13] , Tian Li[14] , the submerged water jet vertical sand flushing simulation verification experiments were carried out, and the geometric model is shown in Fig. 1.

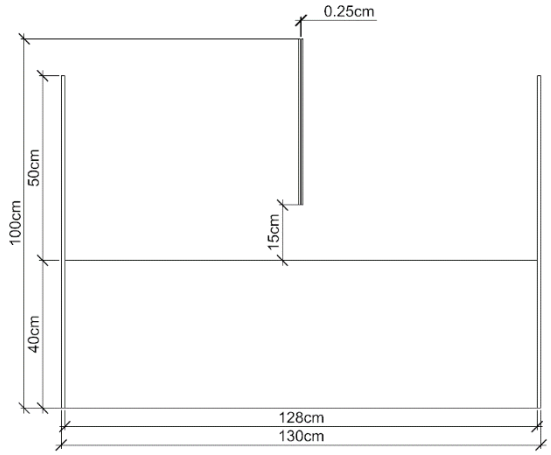

Fig. 1 Geometric model

The overall dimensions of the geometric model are $130cm * 100cm$, the thickness of the deposited sand $40cm$. The nozzle is placed in the middle of the model, and the outlet diameter is taken to be $D = 2.5mm$, the jet target distance is $15cm$. In order to make the experimental data convenient for analysis, take the initial sand plane $Z = 0cm$, with this as a benchmark, set the initial water level height $Z = 50cm$.

The simulation was performed for a total of $10s$, the initial liquid level height $0.5m$, and hydrostatic pressure was used. Regarding the sediment, with reference to the previous experimental data, selected sediment median particle size $d_{50} = 1.8mm$, density $\rho = 2650\text{kg}/m^3$, the maximum sediment deposition fraction $C_V = 0.5$, the angle of rest underwater is $\varphi = 45°$.

3.2 Nested meshing and boundary condition setting

In performing the meshing, it was found that previous authors have used a single grid block division to adjust the size of the grid by adding fixed points in three directions and setting the grid size and number, which reduces the number of grid blocks and makes it possible to calculate fewer boundaries for iterations, but there are some problems as follows:

1) when performing the boundary condition setting, it is not an accurate representation and solid structures need to be added to constrain it. 2) although the program accepts X, Y, Z directions to make cuts with different mesh sizes, but when the mesh aspect ratio is too high, the calculation is prone to non-convergence, which may cause numerical errors. 3) For the symmetric model in this paper, it can be found through pre-experiments that the jet is not a completely vertical jet, but there is a leftward or rightward inclination, as shown in Fig. 2. And the inclination of the jet will dissipate part of the vertical energy, which makes the effect of punching the pit weaker and cannot reach the expected value of the theory, and because the deflection of the jet will make the pit shape also become irregular, and the left and right deviations are large, so that the measured parameters cannot express the effect of the pit punching well.

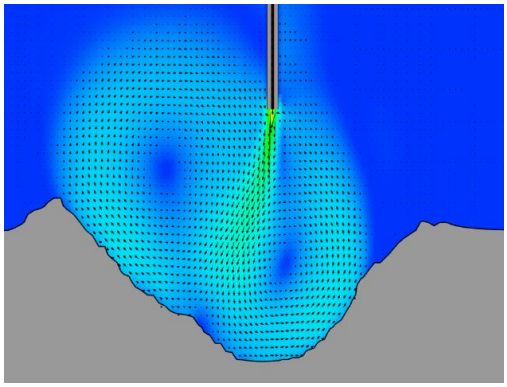

Fig. 2 Tilt phenomenon of vertical jet

In this paper, a total of two meshing schemes are used based on the previous ideas:

1) using nested meshes, for the main region, after considering the computational accuracy and efficiency, the main cell mesh size is selected as $1cm$. Add six fixed points at the outer wall of the nozzle and at the overflow plate, and the grid size in the X direction grew gradually from the center to both sides. In the Z direction, three fixed points were added at the outlet plane, initial sand plane, and static horizontal plane of the nozzle. New nozzle grid blocks are added and meshing it separately. The grid division results are shown in Fig. 3, and the total number of grid cells is 16225.

2) A nested grid is used, and different from the first set of grids, the second set of grids only cover one side of the model($X \geq 0$). And without affecting the premise of the punch pit, the appropriate increase in the outer wall thickness of the nozzle to adapt to the nested grid boundary matching conditions, the grid division results are shown in Fig. 4. The total number of grid cells is 7670.

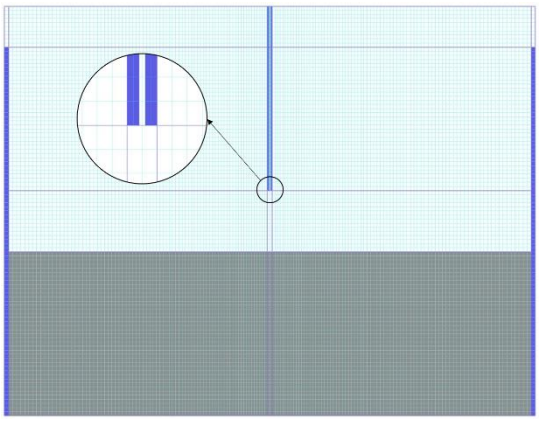

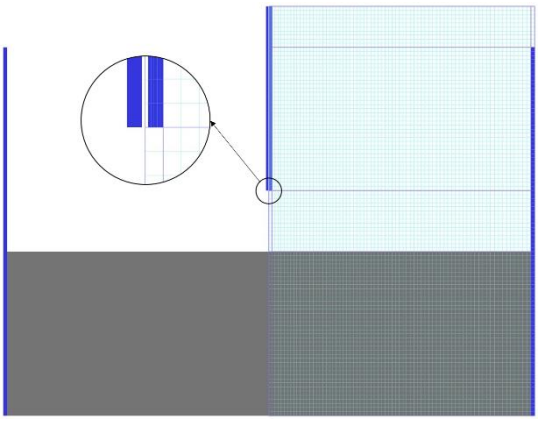

Fig. 3 Schematic diagram of grid division of option 1 Fig. 4 Schematic diagram of grid division of option 2

The boundary conditions are set in Table 1.

Table 1 Boundary condition setting

	Main area grid block		Nozzle area grid block	
Option I	X	Specified pressure boundary. Fluid elevation 0.5m.	X	Grid block boundaries. $Symmetry.$
	Y	Symmetric boundaries. $Symmetry.$	Y	Symmetric boundaries. $Symmetry.$
	Z_{min}	No slippery wall surfaces. $Wall.$	Z_{min}	Grid block boundaries. $Symmetry.$
	Z_{max}	Specified pressure boundary. Fluid fraction is 0.	Z_{max}	Specified velocity boundary. $V_Z = -5m/s.$
Option II	X_{min}	symmetric boundaries. $Symmetry.$	X_{min}	Symmetric boundaries. $Symmetry.$
	X_{max}	Specified pressure boundary. Fluid elevation 0.5m.	X_{max}	Grid block boundaries. $Symmetry.$
	Y	Symmetric boundaries. $Symmetry.$	Y	Symmetric boundaries. $Symmetry.$
	Z_{min}	No slippery wall surfaces. $Wall.$	Z_{min}	Grid block boundaries. $Symmetry.$
	Z_{max}	Specified pressure boundary. Fluid fraction is 0.	Z_{max}	Specified velocity boundary. $V_Z = -5m/s.$

Due to the symmetry of jet scour, this paper studies the effect of target distance on the profile of the sand pit from a two-dimensional perspective[5]~[7], and simplifies the three-dimensional model into a two-dimensional model, which greatly reduces the computational effort.

3.3 Validation of results

The depth of scour pit is an important index to measure scour pit[15]~[18]. The change of scour depth with time is shown in Fig. 5.

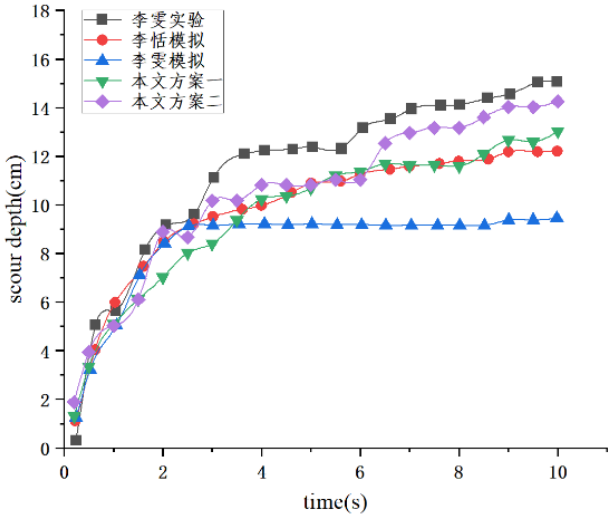

Fig. 5 Variation Trend of maximum scour depth with time

In general, both experimentally and in simulation, the maximum washout pit depth tends to grow logarithmically with time, i.e., at the beginning of the washout, the pit depth increases rapidly in a short period of time, and then the growth rate gradually slows down. In Wen Li's[9] experiment, the maximum punching pit depth grew rapidly to 12.1cm within 0~3.6s, and then the speed slowed down and continued to grow to 15.1cm. The simulated results were in good agreement in the early stage, but after $t > 2.6s$, the maximum pit depth basically stabilized at 9.2cm and did not change anymore, which was much different from the actual experiment. In the numerical simulation of Li Tian [10], the maximum pit depth in 0~2.6s basically matches the experimental results and grows rapidly to 9.2cm, and then the growth rate slows down after $t > 2.6s$, which is not as fast as the experimental one but still continues to grow, and grows to 12.2cm when $t = 10s$, and its growth curve matches the experimental results more closely.

Scenario I of this paper, as can be seen from Fig. 6, the maximum pit depth growth curve basically overlaps with the numerical simulation results of Li Tian, especially in $t > 8s$, slightly better than the simulation results of the previous authors. Scheme II is based on Scenario I to do the grid expression only for the side of $X \geq 0$, thus avoiding the phenomenon of the jet swaying from side to side. It can be found that the curves of Scheme II are more consistent with the experimental results than those of other numerical simulations. Although when $t > 2.6s$ The growth rate after is still not as fast as the experiment, but it can keep a high consistency with the experimental growth trend, which is not achieved by the previous numerical simulation. At $t = 10s$, the maximum washout pit depth reaches 14.2cm. The error of the final result is smaller than that of Li Tian's[10] simulation at 13%.

From the above analysis, it can be concluded that the submerged water jet model established in this paper can better represent the scouring process, and the computational results obtained by using nested grids and expressing only for the side of $X \geq 0$ are more consistent with the experimental results, so the gridding idea is feasible and credible.

4. Numerical simulation of the effect of target distance variables on scouring characteristics

In the previous simulation, it was found that the presence of the side walls also affects the scouring of the jets, In the actual seabed scouring operation，the fluid area is the whole sea area, so the return flow of the jets should not be disturbed by the wall surface. Therefore, the model needs to be further optimized. Adjusting the size of the model to $160cm * 100cm$，the grid division of the model refers to the idea of the Scheme II, grid expression only for the side of $X \geq 0$, based on the previous grid division, new $X = 0.8m$ fixed points are added, the grid size of the cell is still $1cm$. The mesh division is shown in Fig. 6, and the boundary conditions are the same as Scheme II in Table 1.

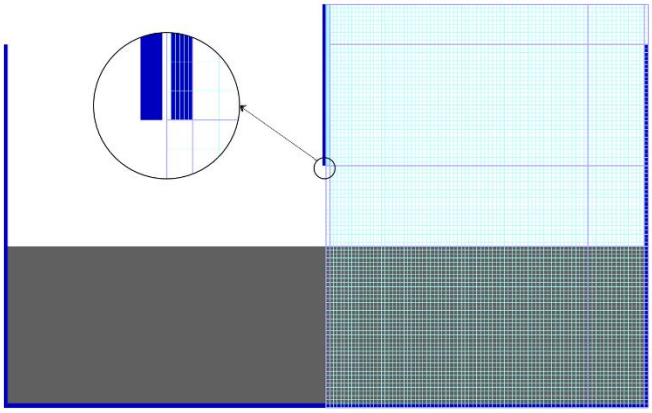

Fig. 6 Schematic diagram of the grid division

According to the literature, the size of jet scour pit is negatively correlated with the particle size of sediment[19]~[20], and positively correlated with the diameter of nozzle outlet[21]. In order to make the scouring effect more obvious, the sediment particle size is selected $d_{50} = 0.9mm$, density $\rho = 2650\text{kg}/m^3$, the maximum sediment deposition fraction $C_V = 0.5$, the angle of rest underwater is $\varphi = 45°$. Take the outlet jet diameter $D = 3mm$.

The simulation is carried out for a total of 100s, and the target distance $l = 15cm$ as an example to illustrate the morphological changes of the punch pit, Fig. 7 is a schematic diagram of the variation of the punch pit profile with time for the working condition of the target distance $l = 15cm$.

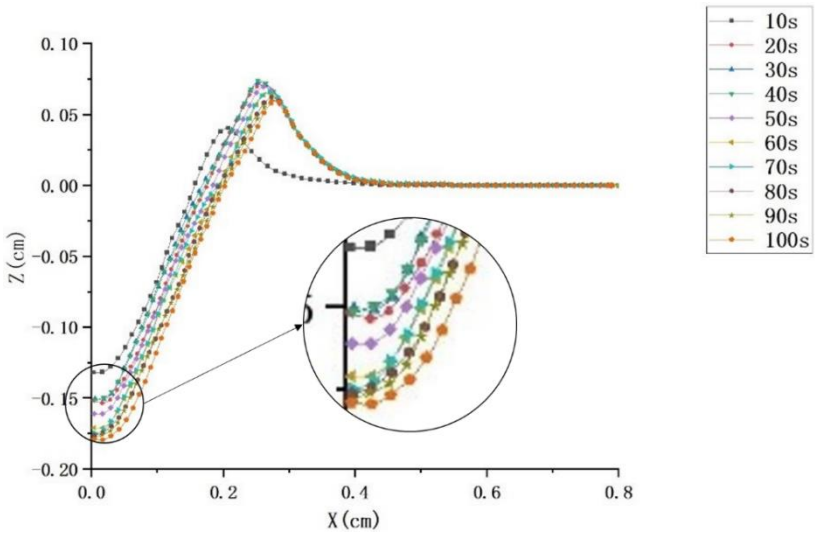

Fig. 7 Schematic diagram of the variation of the punch pit profile with time for the working condition of the target distance $l = 15cm$

From Fig. 7, it can be seen that the profile of the scour pit has an overall increasing trend with the increase of time especially $0\sim10s$ the fastest growth rate within the $10s\sim20s$ The growth continues, but the rate slows down. After 20s, the profile of the scour pit was maintained within a certain range with slight fluctuations up and down, while after 50s, the scouring was almost static, and the profile of the scour pit almost stopped changing with time growth. Through the pre-experiment, it is found that the profile of the scour pit of each group conforms to this rule. After considering the efficiency of scouring and the error of measurement, $t = 30s$ was chosen as the end time of this paper.

Using the depth of the punch pit as a parameter to measure the punch pit[8], Figure 8 shows the depth of the punch pit at the end of each group.

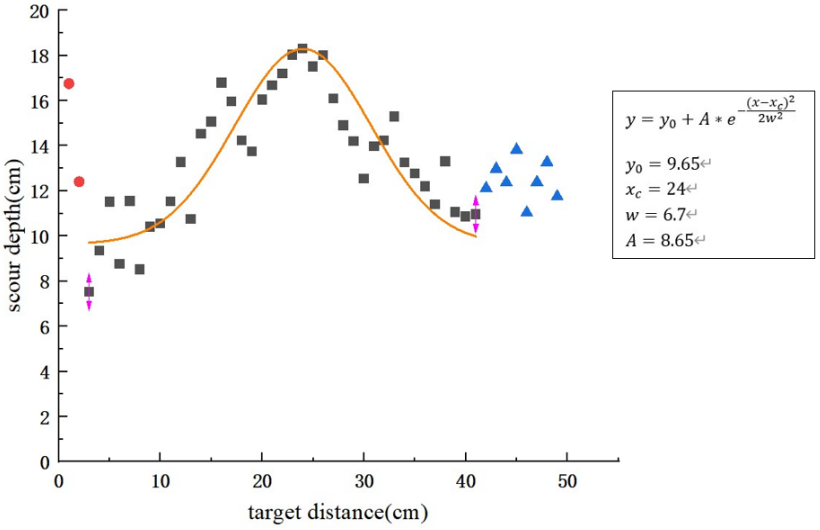

Fig. 8 Depth of scour pit for 30s under various working conditions

It can be seen from fig.8 that when the scouring time is 30s, with the increase of target distance, the maximum scour depth decreases at first, then increases and then decreases. When the target distance is very small, there is almost no energy loss when the jet reaches the sand level, and the depth of the scour pit is large. However, with the increase of the target distance, the depth of the scour pit decreases rapidly. From the suspended sediment concentration (Fig. 9), a large amount of suspended sediment accumulates above the scour pit, the suspended load sinks under the action of gravity and covers the pit wall, which makes the maximum depth of scour pit decrease, which is about the target distance $l = 10cm$ a minimum value is obtained.

After passing through the minimum point, the maximum depth of the scour increases with the increase of the target distance and takes a maximum value at $l = 25cm$. In this process, the starting effect of the vertical jet matches well with that of the horizontal diversion, the generated vortex is small，and the suspended load is transported far enough to sink, forming a flat and regular pit wall. Fig. 10 shows the graph of suspended sand concentration at the target distance $l = 20cm$, and it can be found that the suspended sediment concentration is obviously reduced and evenly distributed on the pit wall.

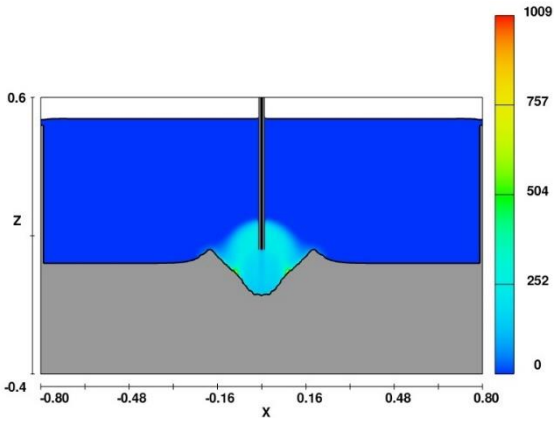

Fig. 9 $l = 5cm$ Suspended sand concentration

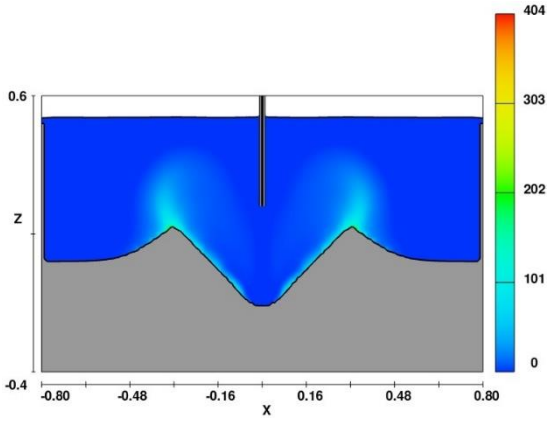

Fig. 10 $l = 5cm$ Suspended sand concentration

After the maximum point, the maximum scour depth decreases with the increase of target distance. When the target distance is too large ($l > 40cm$), at this time, the scouring effect of the jet has been greatly weakened, combined with the actual situation, when the target distance is large, the scouring of the jet is more to cause the ruggedness of the sediment rather than scouring sediment, so the maximum punching scour depth starts repeatedly. Before reaching the sand level, the jet dissipates seriously, and there is no enough energy to start a large amount of sediment, and the amount of suspended sediment is reduced, the suspended sediment also moved to both sides with the larger horizontal diversion，as shown in Fig. 11. The concentration of suspended sediment in this stage is low and mainly distributed near the accumulated sand dunes.

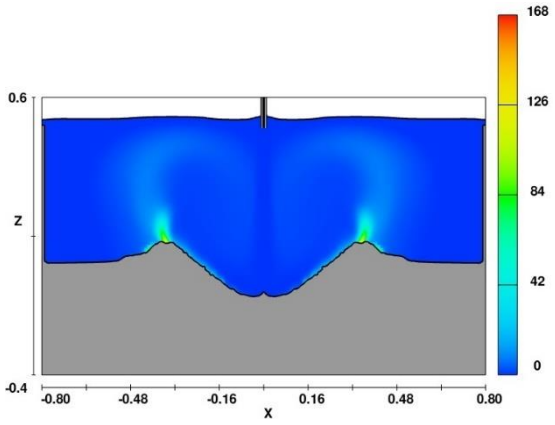

Fig. 11 $l = 49cm$ **Suspended sand concentration**

Except for the cases when the target distance is very small and the target distance is large, the maximum scour depth basically follows the trend of a peak-shaped function, and the empirical formula of the variation of the maximum scour depth with the target distance can be derived by using the method of scatter-fitting curve, as shown in Figure 8.

$$y = y_0 + A * e^{-\frac{(x-x_c)^2}{2w^2}} \tag{9}$$

Where x is the target distance, and y is the maximum depth of the punch pit, $y_0 = 9.65;\ x_c = 24;\ w = 6.7\ ;\ \mathrm{A} = 8.65.$

5. Summary

In this paper, a simulation study of sand flushing experiments with submerged water jets is carried out based on Flow-3D fluid software. First of all, the simulation of sand scouring by predecessors is verified, and a new grid generation idea is proposed. Through comparison, it is found that the calculation results obtained by using nested grid and only expressing the model on one side are more consistent with the results of the physical experiments, and the error is about 13% smaller than that of the previous simulations, which proves the feasibility and credibility of the gridding idea. Then, combined with the idea of nested grid, the simulation experiments of submerged water jet with different target distance variables are carried out. Through the analysis of experimental results, the maximum depth of the scour decreases at first, then increases and then decreases with the change of target distance, and the causes of its formation were briefly analyzed from the perspective of the concentration of suspended sand. Finally, the empirical formula of the peak function of the main section is obtained by the scattered point fitting method. The conclusion can provide guidance for the practical application of water jet under specific conditions.

Author's Biography

Chen Hao, male, master's degree student, research direction: maritime safety technology.

Corresponding author: Teng Xian-bin, male, professor, senior chief engineer, research interests: ship and ocean engineering.

Project Source: Guangdong Provincial Education Department Project (C2206001042)

References

[1] RouseH. Criteria for Similarity in the Transportation of Sediment[J]. University of Iowa Studies in

Engineering，1940．

[2] Dunn I S．Tractive resistance of cohesive channels[J]．1959：85．

[3] Rajaratnam N．Erosion by submerged circular jets．[J]．Journal of the Hydraulics Division，1982，108(2)：262-267．

[4] Aderibigbe，N．Rajaratnam．Erosion of loose beds by submerged circular impinging vertical turbulent jets[J]．Journal of Hydraulic Research，1996．34(1)：19-33．

[5] F. Mercier, F. Golay, S. Bonelli, F. Anselmet, R. Borghi, P. Philippe. 2D axisymmetrical numerical modelling of the erosion of a cohesive soil by a submerged turbulent impinging jet[J]. European Journal of Mechanics / B Fluids,2014,45.

[6] Zhiyuan Yue, Qingquan Liu, Wei Huang, Peng Hu, Zhixian Cao. A 2D well-balanced, coupled model of water flow, sediment transport, and bed evolution based on unstructured grids with efficient variable storage strategy[J]. International Journal of Sediment Research,2020.

[7] Hongliang Wang, Zhongdong Qian, Di Zhang, Tao Wang, Chuan Wang. Numerical Study of the Normal Impinging Water Jet at Different Impinging Height, Based on Wray–Agarwal Turbulence Model[J]. Energies,2020,13(7).

[8] Jiaoyi Hou, Lishan Zhang, Yongjun Gong, Dayong Ning, Zengmeng Zhang. Theoretical and experimental study of scour depth by submerged water jet[J]. Advances in Mechanical Engineering,2016,8(12).

[9] Liu Cheng, He Yun, Wei He-ping. Study of circular jet flushing to loosen silty sand [J]. Sediment Research, 2001(3): 40-45. (Chinese)

[10] Wang Jian-jun, Ni Fu-sheng. Numerical simulation of two-dimensional vertical submerged jet scouring coarse sand bed [J]. Science, Technology and Engineering, 2014. 14(1): 108-111. (Chinese)

[11] Zhang Li-shan. Research on the design and working mechanism of deep-sea mud flushing operation device [D]. Master's thesis, Dalian Maritime University, 2017. (Chinese)

[12] Liu, Cheng-Lin, Chen, Yu-Hao. Numerical simulation of horizontal jet scouring sediment based on Flow-3D[J]. People's Changjiang,2016,47(06):87-91. (Chinese)

[13] Li Wen, Ni Fu-sheng, Wang Jian-jun. Numerical simulation of the effect of target distance on sand bed scouring by submerged jets[J]. Science Technology and Engineering,2014,14(29):290-294. (Chinese)

[14] Li Tian. Numerical simulation of jet scouring characteristics of underwater mixing nozzle[D]. Xi'an University of Technology, 2021. (Chinese)

[15] Sun Cheng-yu. Numerical simulation of underwater jet scour [D]. Huazhong University of Science and Technology,2018. (Chinese)

[16] Huang Jia-li, Ni Fu-sheng, Gu Lei. Study of FLOW-3D numerical method for sediment scour simulation[J]. China Harbor Construction,2019,39(10):6-11. (Chinese)

[17] Zhang Hao, Ni Fu-sheng, Gu Lei. Experimental study of vertical scouring pit depth of jet at a certain target distance[J]. Science Technology and Engineering,2014,14(02):238-240. (Chinese)

[18] Huai W.X., Wang Z.W., Qian Z.D., et al. Numerical simulation of two-dimensional vertical jet sandy riverbed scour [J]. Chinese Science: Technical Science, 2012. 42(1): 72-81. (Chinese)

[19] Liu S.-Y. Effect of sediment particle size and jet velocity on sand bed scouring [J]. Human Name Changjiang. 2017, 48(23): 79-84. (Chinese)

[20] Zhong Liang, Xu Guang-xiang, Zeng Feng. Fractal expression of the equivalent roughness of sand grains[J]. Advances in Water Science,2013,24(01):111-117. (Chinese)

[21] Liu Xiao-Liang, Gao Hui, Jiao Xiang-Dong, Tian Lu. Numerical simulation of high-pressure water jet in submerged environment based on FLUENT[J]. Mechanical Design and Manufacture,2016(11):117-120. (Chinese)